Studies of dust and gas in the interstellar medium of the Milky Way

Salgado Cambiazo, F.J.

Chapter 4

Low Frequency Carbon Radio Recombination Lines I: Calculations of Departure Coefficients

Based on: Salgado, F. et al., 2015

Abstract

In the first paper of this series, we study the level population problem of recombining carbon ions. We focus our study on high quantum numbers anticipating observations of Carbon Radio Recombination Lines to be carried out by the LOw Frequency ARray (LOFAR). We solve the level population equation including angular momentum levels with updated collision rates up to high principal quantum numbers. We derive departure coefficients by solving the level population equation in the hydrogenic approximation and including low temperature dielectronic recombination effects. Our results in the hydrogenic approximation agree well with those of previous works. When comparing our results including dielectronic recombination we find differences mainly due to differences in the collision rates. A comparison with observations is discussed in an accompanying article, as radiative transfer effects need to be considered.

4.1 Introduction

The interplay of stars and their surrounding gas leads to the presence of distinct phases in the interstellar medium (ISM) of galaxies (e.g. Field et al. 1969; McKee and Ostriker 1977). Diffuse atomic clouds (the Cold Neutral Medium, CNM) have densities of about 50 cm^{-3} and temperatures of about 80 K, where atomic hydrogen is largely neutral but carbon is singly ionized by photons with energies between 11.2 eV and 13.6 eV. The warmer ($\sim$ 8000 K) and more tenuous ($\sim$ 0.5 cm^{-3}) intercloud phase is heated and ionized by FUV and EUV photons escaping from HII regions (Wolfire et al., 2003), usually referred to as the Warm Neutral medium (WNM) and Warm Ionized Medium (WIM). The phases of the ISM are often globally considered to be in thermal equilibrium and in pressure balance (Savage and Sembach, 1996; Cox, 2005). However, the observed large turbulent width and presence of gas at thermally unstable, intermediate temperatures attests to the importance of heating by kinetic energy input. In addition, the ISM also hosts molecular clouds, where hydrogen is in the form of H_2 and self-gravity plays an important role. All of these phases are directly tied to key questions on the origin and evolution of the ISM, including the energetics of the CNM, WNM and the WIM; the evolutionary relationship of atomic and molecular gas; the relationship of these ISM phases with newly formed stars; and the conversion of their radiative and kinetic power into thermal and turbulent energy of the ISM (e.g. Cox 2005; Elmegreen and Scalo 2004; Scalo and Elmegreen 2004; McKee and Ostriker 2007).

The neutral phases of the ISM have been studied using optical and UV observations of atomic lines. These observations can provide the physical conditions but are limited to pinpoint experiments towards bright background sources and are hampered by dust extinction (Snow and McCall, 2006). At radio wavelengths, dust extinction is not important and observations of the 21 cm hyperfine transition of neutral atomic hydrogen have been used to study the neutral phases (e.g. Weaver and Williams 1973; Kalberla et al. 2005; Heiles and Troland 2003b). On a global scale, these observations have revealed the prevalence of the two phase structure in the interstellar medium of cold clouds embedded in a warm intercloud medium but they have also pointed out challenges to this theoretical view (Kulkarni and Heiles, 1987; Kalberla and Kerp, 2009). It has been notoriously challenging to determine the physical characteristics (density, temperature) of the neutral structures in the ISM as separating the cold and warm components is challenging (e.g. Heiles and Troland 2003a). In this context, Carbon radio recombination lines (CRRLs) provide a promising tracer of the neutral phases of the ISM (e.g. Peters et al. 2011; Oonk et al. 2015b).

Carbon has a lower ionization potential (11.2 eV) than hydrogen (13.6 eV)

and can be ionized by radiation fields in regions where hydrogen is largely neutral. Recombination of carbon ions with electrons to high Rydberg states will lead to CRRLs in the sub-millimeter to decameter wavelength range. Carbon radio recombination lines have been observed in the interstellar medium of our Galaxy towards two types of clouds: diffuse clouds (e.g.: Konovalenko and Sodin 1981; Erickson et al. 1995; Roshi et al. 2002; Stepkin et al. 2007; Oonk et al. 2014) and photodissociation regions (PDRs), the boundaries of HII regions and their parent molecular clouds (e.g.: Natta et al. 1994; Wyrowski et al. 1997; Quireza et al. 2006). The first low frequency (26.1 MHz) carbon radio recombination line was detected in absorption towards the supernova remnant Cas A by Konovalenko and Sodin (1980) (wrongly attributed to a hyperfine structure line of ^{14}N, Konovalenko and Sodin 1981). This line corresponds to a transition occurring at high quantum levels ($n = 631$). Recently, Stepkin et al. (2007) detected CRRLs in the range 25.5–26.5 MHz towards Cas A, corresponding to transitions involving levels as large as $n = 1009$.

Observations of low frequency carbon recombination lines can be used to probe the physical properties of the diffuse interstellar medium. However, detailed modeling is required to interpret the observations. Watson et al. (1980); Walmsley and Watson (1982a) showed that, at low temperatures ($T_e \lesssim 100$ K), electrons can recombine into carbon ions by simultaneously exciting the $^2P_{1/2} - {}^2P_{3/2}$ fine structure line, a process known as dielectronic recombination. Such recombination process occurs to high n states, and can explain the behavior of the high n CRRLs observed towards Cas A. Walmsley and Watson (1982a) modified the code from Brocklehurst and Salem (1977) to include dielectronic recombination. Payne et al. (1994) modified the code to consider transitions up to 10000 levels. All of these results assume a statistical distribution of the angular momentum levels, an assumption that is not valid at intermediate levels for low temperatures. Moreover, the lower the temperature, the higher the n-level for which that assumption is not valid.

The increased sensitivity, spatial resolution, and bandwidth of the Low Frequency ARray (LOFAR, van Haarlem et al. 2013) is opening the low frequency sky to systematic studies of high quantum number radio recombination lines. The recent detection of high level carbon radio recombination lines using LOFAR towards the line of sight of Cas A (Asgekar et al., 2013), Cyg A (Oonk et al., 2014), and the first extragalactic detection in the starburst galaxy M82 (Morabito et al., 2014a) illustrate the potential of LOFAR for such studies. Moreover, pilot studies have demonstrated that surveys of low frequency radio recombination lines of the galactic plane are within reach, providing a new and powerful probe of the diffuse interstellar medium. These new observations have motivated us to reassess some of the approximations made by previous works and to expand the range of applicability of recombination line theory in terms of physical parameters. In addition, increased computer power allows us to

solve the level population problem considering a much larger number of levels than ever before. Furthermore, updated collisional rates are now available (Vrinceanu et al., 2012), providing more accurate results. Finally, it can be expected that the Square Kilometer Array, SKA, will further revolutionize our understanding of the low frequency universe with even higher sensitivity and angular resolution (Oonk et al., 2015b).

In this work, we present the method to calculate the level population of recombining ions and provide some exemplary results applicable to low temperature diffuse clouds in the ISM. In Section 5, we will present results specifically geared towards radio recombination line studies of the diffuse interstellar medium. In Section 4.2, we introduce the problem of level populations of atoms and the methods to solve this problem for hydrogen and hydrogenic carbon atoms. We also present the rates used in this work to solve the level population problem. In Section 4.3, we discuss our results focusing on hydrogen and carbon atoms. We compare our results in terms of the departure coefficients with previous results from the literature. In Section 4.4, we summarize our results and provide the conclusions of the present work.

4.2 Theory

A large fraction of our understanding of the physical processes in the Universe comes from observations of atomic lines in astrophysical plasmas. In order to interpret the observations, accurate models for the level population of atoms are needed as the strength (or depth) of an emission (absorption) line depends on the level populations of atoms. Here, we summarize the basic ingredients needed to build level population models and provide a basic description of the level population problem. We begin our discussion by describing the line emission and absorption coefficients (j_ν and k_ν, respectively), which are given by (Shaver, 1975; Gordon and Sorochenko, 2009):

$$j_\nu = \frac{h\nu}{4\pi} A_{n'n} N_{n'} \phi(\nu), \tag{4.1}$$

$$k_\nu = \frac{h\nu}{4\pi} \left(N_n B_{nn'} - N_{n'} B_{n'n} \right) \phi(\nu), \tag{4.2}$$

where h is the Planck constant, $N_{n'}$ is the level population of a given upper level (n') and N_n is the level population of the lower level (n); $\phi(\nu)$ is the line profile, ν is the frequency of the transition and $A_{n'n}$, $B_{n'n}(B_{nn'})$ are the Einstein coefficients for spontaneous and stimulated emission (absorption) [1], respectively.

[1] We provide the formulation to obtain the values for the rates in Appendix C.

Under local thermodynamic equilibrium (LTE) conditions, level populations are given by the Saha-Boltzmann equation (e.g. Brocklehurst 1971):

$$N_{nl}(LTE) \quad = \quad N_e N_{ion} \left(\frac{h^2}{2\pi m_e k T_e} \right)^{3/2} \frac{\omega_{nl}}{2\omega_i} e^{\chi_n}, \chi_n = \frac{hcRyZ^2}{n^2 kT_e}, \quad (4.3)$$

where T_e is the electron temperature, N_e is the electron density in the nebula, N_{ion} is the ion density, m_e is the electron mass, k is the Boltzmann constant, h is the Planck constant, c is the speed of light and Ry is the Rydberg constant; ω_{nl} is the statistical weight of the level n and angular quantum momentum level l [$\omega_{nl} = 2(2l+1)$, for hydrogen], and ω_i is the statistical weight of the parent ion. The factor $\left(h^2/2\pi m_e k T_e\right)^{1/2}$ is the thermal de Broglie wavelength, $\Lambda(T_e)$, of the free electron [2]. In the most general case, lines are formed under non-LTE conditions and the level population equation must be solved in order to properly model the line properties as a function of quantum level (n).

Following e.g. Seaton (1959a) and Brocklehurst (1970), we present the results of our modeling in terms of the departure coefficients (b_{nl}), defined by:

$$b_{nl} = \frac{N_{nl}}{N_{nl}(LTE)}, \quad (4.4)$$

and b_n values are computed by taking the weighted sum of the b_{nl} values:

$$b_n = \sum_{l=0}^{n-1} \left(\frac{2l+1}{n^2} \right) b_{nl}, \quad (4.5)$$

note that, at a given n, the b_{nl} values for large l levels influence the final b_n value the most due to the statistical weight factor. At low frequencies stimulated emission is important (Goldberg, 1966) and we introduce the correction factor for stimulated emission as defined by Brocklehurst and Seaton (1972):

$$\beta_{n,n'} = \frac{1 - (b_{n'}/b_n)\exp(-h\nu/kT_e)}{1 - \exp(-h\nu/kT_e)}, \quad (4.6)$$

unless otherwise stated the β_n presented here correspond to α transitions ($n' = n+1 \rightarrow n$). The description of the level population in terms of departure coefficients is convenient as it reduces the level population problem to a more easily handled problem as we will show in Section 4.2.1.

4.2.1 Level Population of Carbon Atoms under Non-LTE Conditions

The observations of high n carbon recombination lines in the ISM motivated Watson et al. (1980) to study the effect on the level population of dielectronic

[2] $\Lambda(T_e)^3 \approx 4.14133 \times 10^{-16}\ T_e^{-1.5}$ cm^3.

recombination [3] and its inverse process (autoionization) in low temperature ($T_e \lesssim 100$ K) gas. Watson et al. (1980) used l-changing collision rates [4] from Jacobs and Davis (1978) and concluded that for levels $n \approx 250 - 300$, dielectronic recombination of carbon ions can be of importance. In a later work, Walmsley and Watson (1982a) used collision rates from Dickinson (1981) and estimated a value for which autoionization becomes more important than angular momentum changing rates. The change in collision rates led them to conclude that the influence of dielectronic recombination on the b_n values is important at levels $n \gtrsim 300$. Clearly, the results are sensitive to the choice of the angular momentum changing rates. Here, we will explicitly consider l-sublevels when solving the level population equation.

The dielectronic recombination and autoionization processes affect only the C+ ions in the $^2P_{3/2}$ state, therefore we treat the level population for the two ion cores in the $^2P_{1/2}$ separately in the evaluation of the level population (Walmsley and Watson, 1982a). The equations for carbon atoms recombining to the $^2P_{3/2}$ ion core population have to include terms describing dielectronic recombination (α^d_{nl}) and autoionization (A^a_{nl}), viz.:

$$b_{nl}\left[\sum_{n'<n}\sum_{l'=l\pm1} A_{nln'l'} + \sum_{n'\neq n}(B_{nln'l'}I_\nu + C_{nln'l'}) + \sum_{l'=l\pm1} C_{nlnl'} + A^a_{nl} + C_{nl,i}\right] =$$
$$\sum_{n'>n}\sum_{l'=l\pm1} b_{n'l'}\frac{\omega_{n'l'}}{\omega_{nl}}e^{\Delta\chi_{n'n}}A_{n'l'nl} + \sum_{n'\neq n}\sum_{l'=l\pm1} b_{n'l'}\frac{\omega_{n'l'}}{\omega_{nl}}e^{\Delta\chi_{n'n}}(B_{n'l'nl}I_\nu + C_{n'l'nl}) +$$
$$+\sum_{l'=l\pm1} b_{nl'}\left(\frac{\omega_{nl'}}{\omega_{nl}}\right)C_{nl'nl} + \frac{N_eN^+_{3/2}}{N_{nl}(LTE)}(\alpha_{nl} + C_{i,nl}) + \frac{N_eN^+_{1/2}}{N_{nl}(LTE)}\alpha^d_{nl}. \quad (4.7)$$

The left hand side of Equation 4.7 describes all the processes that take an electron out of the nl-level, and the right hand side the processes that add an electron to the nl level; $A_{nln'l'}$ is the coefficient for spontaneous emission, $B_{nln'l'}$ is the coefficient for stimulated emission or absorption induced by a radiation field I_ν; $C_{nln'l'}$ is the cross section for energy changing collisions (i.e. transitions with $n \neq n'$), $C_{nlnl'}$ is the coefficient for l-changing collisions; $C_{nl,i}$ ($C_{i,nl}$) is the coefficient for collisional ionization (3-body recombination) and α_{nl} is the coefficient for radiative recombination. A description of the coefficients entering in Equation 4.7 is given in Section 4.2.3 and in further detail in the Appendix. The level population equation is solved by finding the values for the departure coefficients. The level population for carbon ions recombining to the

[3] Recombination to a high n state accompanied by the simultaneous excitation of the $^2P_{1/2}$ C+ electron to the $^2P_{1/2}$ state.

[4] We use the term l-changing collision rates to refer to collisions rate that induce a transition from state nl to $nl \pm 1$

$^2P_{1/2}$ level is hydrogenic and we solve for the departure coefficients ($b_{nl}^{1/2}$) using Equation 4.7, but ignoring the coefficients for dielectronic recombination and autoionization.

After computing the $b_{nl}^{1/2}$ and $b_{nl}^{3/2}$, we compute the departure coefficients ($b_n^{1/2}$ and $b_n^{3/2}$) for both parent ion populations by summing over all l-states (Equation 4.5). The final departure coefficients for carbon are obtained by computing the weighted average of both ion cores:

$$b_n^{final} = \frac{b_n^{1/2} + b_n^{3/2}\left[N_{3/2}^+/N_{1/2}^+\right]}{1+\left[N_{3/2}^+/N_{1/2}^+\right]}. \tag{4.8}$$

Note that, in order to obtain the final departure coefficients, the relative population of the parent ion cores is needed. Here, we assume that the population ratio of the two ion cores $N_{3/2}^+$ to $N_{1/2}^+$ is determined by collisions with electrons and hydrogen atoms. This ratio can be obtained using (Ponomarev and Sorochenko, 1992; Payne et al., 1994):

$$R = \frac{N_{3/2}^+/N_{1/2}^+}{N_{3/2}^+(LTE)/N_{1/2}^+(LTE)} \tag{4.9}$$

$$= \frac{N_e\gamma_e + N_H\gamma_H}{N_e\gamma_e + N_H\gamma_H + A_{3/2,1/2}}, \tag{4.10}$$

where $\gamma_e = 4.51\times10^{-6}\ T_e^{-1/2}$ cm^{-3} s^{-1} is the de-excitation rate due to collisions with electrons, $\gamma_H = 5.8\times10^{-10}\ T_e^{0.02}$ cm^{-3} s^{-1} is the de-excitation rate due to collisions with hydrogen atoms (Payne et al., 1994) [5], $N_{\rm H}$ is the atomic hydrogen density and $A_{3/2,1/2} = 2.4\times10^{-6}$ s^{-1} is the spontaneous radiative decay rate of the core. In this work, we have ignored collisions with molecular hydrogen, which should be included for high density PDRs. Collisional rates for H_2 excitation of C^+ have been calculated by Flower (1988). In the cases of interest here, the value of R is dominated by collisions with atomic hydrogen. We recognize that the definition of R given in Equation 4.9 is related to the critical density (N_{cr}) of a two level system by $R = 1/(1+N_{cr}/N_X)$ where N_X is the density of the collisional partner (electron or hydrogen). The LTE ratio of the ion core is given by the statistical weights of the levels and the temperature

[5]Payne et al. (1994) used rates from Tielens and Hollenbach (1985), based on Launay and Roueff (1977) for collisions with hydrogen atoms and Hayes and Nussbaumer (1984) for collisions with electrons. Newer rates are available for collisions with electrons (Wilson and Bell, 2002) and hydrogen atoms (Barinovs et al., 2005), but the difference in values is negligible.

(T_e) of the gas:

$$\frac{N^+_{3/2}(LTE)}{N^+_{1/2}(LTE)} = \frac{g_{3/2}}{g_{1/2}} e^{-\Delta E/kT_e}, \tag{4.11}$$

where $g_{3/2} = 4$, $g_{1/2} = 2$ are the statistical weights of the fine structure levels and $\Delta E = 92$ K is the energy difference of the fine structure transition. The LTE level population ratio as a function of temperature is shown in Figure 4.1, illustrating the strong dependence on temperature of this value. At densities below the critical density (≈ 300 cm^{-3} for collisions with H), the fine structure levels fall out of LTE and the value for R becomes very small (Figure 4.1). Note that R is not very sensitive to the temperature.

With the definition of R given above, the final departure coefficient can be written as (Ponomarev and Sorochenko, 1992):

$$b_n^{final} = \frac{b_n^{1/2} + b_n^{3/2} R \left[N^+_{3/2}/N^+_{1/2}\right]_{LTE}}{1 + R \left[N^+_{3/2}/N^+_{1/2}\right]_{LTE}}. \tag{4.12}$$

The final departure coefficient is the value that we are interested in to describe CRRLs.

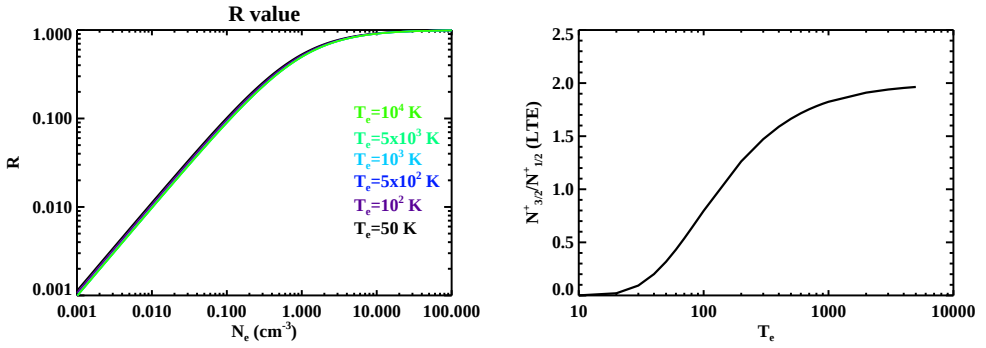

Figure 4.1: Left panel: R value as a function of electron temperature, in a range of densities. The R value is nearly independent of temperature, and for $N_e > 10$ cm^{-3}, $R \approx 1$. Right panel: ion "LTE" ratios as a function of T_e, independent of density.

4.2.2 Numerical Method

Having described how to derive the b_n^{final}, now we focus on the problem of obtaining the departure coefficients for both ion cores from the level population

equation. We use the same procedure to obtain the departure coefficients for both parent ion cores, as the only difference in the level population equation for the $^2P_{3/2}$ and the $^2P_{1/2}$ cores is the inclusion of dielectronic recombination and autoionization processes. We will refer as b_{nl} and b_n without making a distinction between the $^2P_{3/2}$ and $^2P_{1/2}$ in this subsection.

We follow the methods described in Brocklehurst (1971) and improved in Hummer and Storey (1987) to solve the level population equation in an iterative manner. First, we solve the level population equation by assuming that the l sublevels are in statistical equilibrium, i.e. $b_n = b_{nl}$ for all l sublevels. We refer to this approach as the n-method (see Appendix B). Second, we used the previously computed values to determine the coefficients on the right hand side of Equation 4.7 that contain terms with $n' \neq n$. Thus, the level population equation for a given n is a tridiagonal equation on the l sublevels involving terms of the type $l \pm 1$. This tridiagonal equation is solved for the b_{nl} values (further details are given in Appendix B). The second step of this procedure is repeated until the difference between the computed departure coefficients is less than 1%.

We consider a fixed maximum number of levels, n_{max}, equal to 9900. We make no explicit assumptions on the asymptotic behavior of the b_n for larger values of n. Therefore, no fitting or extrapolation is required for large n. The adopted value for n_{max} is large enough for the asymptotic limit – $b_n \to 1$ for $n > n_{max}$ – to hold even at the lowest densities considered here. For the nl-method, we need to consider all l sublevels up to a high level ($n \sim 1000$). For levels higher than this critical n level (n_{crit}), we assume that the l sublevels are in statistical equilibrium. In our calculations $n_{crit} = 1500$, regardless of the density.

4.2.3 Rates Used in this Work

In this section, we provide a brief description of the rates used in solving the level populations. Further details and the mathematical formulations for each rate are given in Appendices C, D, E and F. Accurate values for the rates are critical to obtain meaningful departure coefficients when solving the level population equation (Equation 4.7). Radiative rates are known to high accuracy ($< 1\%$) as they can be computed from first principles. On the other hand, collision rates at low temperatures are more uncertain ($\sim 20\%$, Vriens and Smeets 1980).

4.2.3.1 Einstein A and B coefficient

The Einstein coefficients for spontaneous and stimulated transitions can be derived from first principles. We used the recursion formula described in Storey

and Hummer (1991) to obtain the values for the Einstein $A_{nln'l'}$ coefficients. To solve the n method (our first step in solving the level population equation) we require the values for $A_{nn'}$, which can be easily obtained by summing the $A_{nln'l'}$:

$$A_{nn'} = \frac{1}{n^2}\sum_{l'=0}^{n-1}\sum_{l=l'\pm1}(2l+1)A_{nln'l'}. \tag{4.13}$$

The mathematical formulation to obtain values for spontaneous transitions is detailed in Appendix C.

The coefficients for stimulated emission and absorption ($B_{nn'}$) are related to the $A_{nn'}$ coefficients by:

$$B_{nn'} = \frac{c^2}{2h\nu^3}A_{nn'}, \tag{4.14}$$

$$B_{n'n} = \left(\frac{n}{n'}\right)^2 B_{nn'}. \tag{4.15}$$

4.2.3.2 Energy changing collision rates

In general, energy changing collisions are dominated by the interactions of electrons with the atom. The interaction of an electron with an atom can induce transitions of the type:

$$X_{nl} + e^- \rightleftarrows X_{n'l'} + e^-, \tag{4.16}$$

with $n' \neq n$ changing the distribution of electrons in an atom population. Hummer and Storey (1987) used the formulation of Percival and Richards (1978). The collision rates derived by Percival and Richards (1978) are essentially the same as Gee et al. (1976). However, the collision rates from Gee et al. (1976) are not valid for the low temperatures of interest here. Instead, we use collision rates from Vriens and Smeets (1980). We note that at high T_e and for high n levels, the Bethe (Born) approximation holds and values of the rates from Vriens and Smeets (1980) differ by less than 20% when compared to those from Gee et al. (1976). The good agreement between the two rates is expected since the results from Vriens and Smeets (1980) are based on Gee et al. (1976). On the other hand, at low T_e and for low n levels values the two rates differ by several orders of magnitude and, indeed, the Gee et al. (1976) values are too high to be physically realistic. A comparison of the rates for different values of T_e and $n \rightarrow n + \Delta n$ transitions is shown in Figure 4.2. We explore the effects of using Vriens and Smeets (1980) rates on the b_n values in Section 4.3.2.

The inverse rates are obtained from detailed balance:

$$C_{n'n} = \left(\frac{n}{n'}\right)^2 e^{\chi_n - \chi_{n'}} C_{nn'}. \tag{4.17}$$

In order to solve the nl-method, rates of the type $C_{nln'l'}$ with $n \neq n'$ are needed. Here, the approach of Hummer and Storey (1987) is followed and the collision rates are normalized by the oscillator strength of the transitions (Equation 5 in Hummer and Storey 1987). Only transitions with $\Delta l = 1$ were included as these dominate the collision process (Hummer and Storey, 1987),.

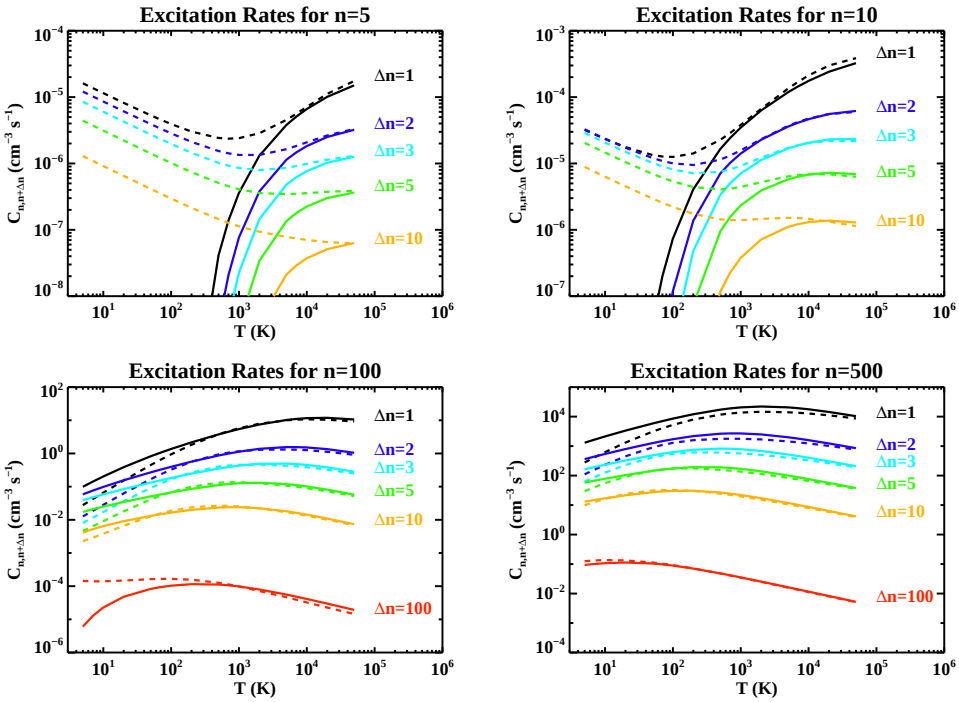

Figure 4.2: Comparison of energy changing collision rates. The dashed lines correspond to the Gee et al. (1976) rates while the solid lines are from Vriens and Smeets (1980). Large differences between Gee et al. (1976) and Vriens and Smeets (1980) can be seen at low T_e and at low n levels. As is well known, transitions with $\Delta n = 1$ dominate. The difference between $\Delta n > 1$ and $\Delta n = 1$ rates is less at lower T_e.

4.2.3.3 Angular momentum changing collision rates

For low n levels, the l level population has to be explicitly calculated. Moreover, for the dielectronic recombination process, the angular momentum changing collisions set the value for which the dielectronic recombination process is important, and transitions of the type:

$$X_{nl} + \mathrm{C}^{+} \rightleftarrows X_{nl\pm1} + \mathrm{C}^{+} \tag{4.18}$$

must be considered. In general, collisions with ions are more important than collisions with electrons. Here, for simplicity, we adopt that C^+ is the dominant cation.

Hummer and Storey (1987) used l-changing collision rates from Pengelly and Seaton (1964) which are computed iteratively for a given n level starting at $l = 0$ or $l = n - 1$. However, as pointed out by Hummer and Storey (1987) and Brocklehurst (1971), the values for the l-changing rates obtained by starting the iterations at $l = 0$ differ from those obtained when starting at $l = n-1$. Moreover, averaging the l-changing rates obtained by the two different initial conditions leads to an oscillatory behavior of the rates that depends on l (Brocklehurst, 1970). Hummer and Storey (1987) circumvented this problem by normalizing the value of the rates by the oscillator strength (Equation 4 in Hummer and Storey 1987). In addition, at high n levels and high densities the values for $C_{nln'l'}$ can become negative (Equation 43 in Pengelly and Seaton 1964). This poses a problem when studying the level population of carbon atoms at the high n levels of interest in the present work[6]. The more recent study of Vrinceanu et al. (2012) provides a general formulation to obtain the value of l-changing transition rates. These new rates use a better approximation for the cut-off radius of the probability of the transition. Furthermore, the rates from Vrinceanu et al. (2012) are well behaved over a large range of temperature and densities and they do not exhibit the oscillatory behavior with l sublevel shown by the Pengelly and Seaton (1964) rates. Therefore, we use the Vrinceanu et al. (2012) rates in this work. Vrinceanu et al. (2012) derived the following expression, valid for $n > 10$ and $n\sqrt{T_e} < 2.4 \times 10^4$ K$^{1/2}$:

$$C_{nl\rightarrow nl+1} = 24\sqrt{\pi}a_0^3\pi cRyn^4\sqrt{\left(\frac{hcRy}{kT_e}\right)\left(\frac{\mu}{m_e}\right)}\left[1-\left(\frac{l}{n}\right)^2\left(\frac{2l+3}{2l+1}\right)\right].$$

where a_0 is the bohr radius and μ is the reduced mass of the system. Values for the inverse process are obtained by using detailed balance:

$$C_{nl+1\rightarrow nl} = \frac{(2l+1)}{(2l+3)}C_{nl\rightarrow nl+1}. \tag{4.19}$$

We note that the l-changing collision rates obtained by using the formula from Vrinceanu et al. (2012) can differ by orders of magnitude with those using Pengelly and Seaton (1964) formulation. We discuss the effect on the final b_n values in Section 4.3.2, where we compare our results with those of Storey and Hummer (1995).

[6]We note that this was not a problem for Hummer and Storey (1987), since they assumed an statistical distribution of the l levels for high n.

4.2.3.4 Radiative Recombination

Radiative ionization occurs when an excited atom absorbs a photon with enough energy to ionize the excited electron. The process can be represented as follows:

$$X_{nl} + h\nu \rightleftarrows X^+ + e^-, \tag{4.20}$$

and the inverse process is radiative recombination. We use the recursion relation described in Storey and Hummer (1991) to obtain values for the ionization cross-section (Appendix D). Values for the radiative recombination (α_{nl}) coefficients were obtained using the Milne relation and standard formulas (e.g. Rybicki and Lightman (1986), Appendix D). The program provided by Storey and Hummer (1991) only produces reliable values up to $n \sim 500$ due to cancellation effects in the iterative procedure. In order to avoid cancellation effects, the values computed here were obtained by working with logarithmic values in the recursion formula. As expected, our values for the rates match those of Storey and Hummer (1991) well.

For the n-method we require the sum of the individual α_{nl} values:

$$\alpha_n = \sum_{l=0}^{n-1} \alpha_{nl}. \tag{4.21}$$

The averaged α_n values agree well with the approximated formulation of Seaton (1959a) to better than 5%, validating our approach.

4.2.3.5 Collisional ionization and 3-body recombination

Collisional ionization occurs when an atom encounters an electron and, due to the interaction, a bound electron from the atom is ionized. Schematically the process can be represented as:

$$X_n + e^- \quad \rightleftarrows \quad X^+ + e^- + e^-. \tag{4.22}$$

The inverse process is given by the 3-body recombination and the value for the 3-body recombination rate is obtained from detailed balance:

$$\begin{aligned} C_{i,n} &= \frac{N_n(LTE)}{N_{ion}N_e} C_{n,i}, \\ &= \left(\frac{h^2}{2\pi m_e kTe}\right)^{3/2} n^2 e^{\chi_n} C_{n,i}, \\ &= \Lambda(T_e)^3 n^2 e^{\chi_n} C_{n,i}. \end{aligned} \tag{4.23}$$

We used the formulation of Brocklehurst and Salem (1977) and compared the values with those from the formulation given by Vriens and Smeets (1980). For levels above 100 and at $T_e = 10$ K, the Brocklehurst & Salem values are a factor of $\lesssim 2$ larger, but the differences quickly decrease for higher temperatures. To obtain the $C_{nl,i}$ that are needed in the *nl*-method, we followed Hummer and Storey (1987) and assumed that the rates are independent of the angular momentum. The mathematical formulation is reproduced in the Appendix F for convenience of the reader.

4.2.3.6 Dielectronic Recombination and Autoionization on Carbon Atoms

The dielectronic recombination process involves an electron recombining into a level n while simultaneously exciting one of the bound electrons (left side of Equation 4.24, below). This state (X_n^*) is known as an autoionizing state. In this autoionizing state, the atom can stabilize either by releasing the recombined electron through autoionization (inverse process of dielectronic recombination) or through radiative stabilization (right hand side of Equation 4.24). Dielectronic recombination and autoionization are only relevant for atoms with more than one electron.

$$X^+ + e^- \rightleftarrows X_{nl}^* \rightarrow X_{n'l'} + h\nu. \tag{4.24}$$

For C^+ recombination, at $T_e \sim 100$ K free electrons in the plasma can recombine to a high n level, and the kinetic energy is transfered to the core of the ion, producing an excitation of the $^2P_{1/2} - {}^2P_{3/2}$ fine-structure level of the C^+ atom core [7] (which has a difference in energy $\Delta E = 92$ K). Due to the long radiative lifetime of the fine-structure transition (4×10^6 s), radiative stabilization can be neglected.

The autoionization rate, A_{nl}^a, was obtained from the approximate expression given in Dickinson (1981):

$$A_{nl}^a = 2.25 \frac{2\pi Ryc}{n^3 \left(0.5 + l\right)^6}. \tag{4.25}$$

The dielectronic recombination rate is obtained by detailed balance:

$$N_{1/2}^+ N_e \alpha_{nl}^d = N_{nl} A_{nl}^a. \tag{4.26}$$

Walmsley and Watson (1982a) defined b_{di} as the departure coefficient when

[7] The process has been referred in the literature as dielectronic-like recombination or dielectronic capture by Watson et al. (1980).

autoionization/dielectronic recombination dominate:

$$\begin{aligned} b_{di} &= \frac{g_{1/2}N^+_{1/2}}{g_{3/2}N^+_{3/2}} \exp\left[-\Delta E/kT_e\right], \\ &= \frac{1}{R}. \end{aligned} \tag{4.27}$$

4.3 Results

The behavior of CRRLs with frequency depends on the level population of carbon via the departure coefficients. We compute departure coefficients for carbon atoms by solving the level population equation using the rates described in Section 4.2.3 and the approach in Section 4.2.2. Here, we present values for the departure coefficients and provide a comparison with earlier studies in order to illustrate the effect of our improved rates and numerical approach. A detailed analysis of the line strength under different physical conditions relevant for the diffuse clouds and the effects of radiative transfer are provided in an accompanying article (Paper II).

4.3.1 Departure Coefficient for Carbon Atoms

The final departure coefficients for carbon atoms (i.e. b_n^{final}) are obtained by computing the departure coefficients recombining from both parent ions, those in the $^2P_{1/2}$ level and those in the $^2P_{3/2}$ level. Therefore, it is illustrative to study the individual departure coefficients for the $^2P_{1/2}$ core, which are hydrogenic, and the departure coefficients for the $^2P_{3/2}$ core separately.

4.3.1.1 Departure Coefficient in the Hydrogenic Approximation

In Figure 4.3 we show example b_n and $b_n\beta_n$ values obtained in the hydrogenic approximation at $T_e = 10^2$ and 10^4 K for a large range in density. The behavior of the b_n values as a function of n can be understood in terms of the rates that are included in the level population equation. At the highest n levels, collisional ionization and three body recombination dominate the rates in the level population equation and the b_n values are close to unity. We can see that as the density increases, collisional equilibrium occurs at lower n levels and the b_n values approach unity at lower levels. In contrast, for the lowest n levels, the level population equation is dominated by radiative processes and the levels drop out of collisional equilibrium. As the radiative rates increase with decreasing n level, the departure coefficients become smaller. We note that differences in the departure coefficients for the low n levels for different

temperatures are due to the radiative recombination rate, which has a $T_e^{-3/2}$ dependence.

At intermediate n levels, the behavior of the b_n as a function of n shows a more complex pattern with a pronounced "bump" in the b_n values for intermediate levels ($n \sim 10$ to ~ 100). To guide the discussion we refer the reader to Figure 4.3. Starting at the highest n, $b_n \to 1$, as mentioned above. For these high n levels, l-changing collisions efficiently redistribute the electron population among the l states and, at high density, the b_{nl} departure coefficients are unity as well (Figure 4.4, upper panels). For lower values of n, the b_n values decrease due to an increased importance of spontaneous transitions. At these n levels, the b_n values obtained by the nl method differ little from the values obtained by the n-method, since l-changing collisions efficiently redistribute the electrons among the l sublevels for a given n level. For lower n levels, the effects of considering the l sublevel distribution become important as l-changing collisions compete with spontaneous decay, effectively "storing" electrons in high l sublevels for which radiative decay is less important. Specifically, the spontaneous rate out of a given level is approximately $A_{nl} \simeq 10^{10}/n^3/l^2(\mathrm{s}^{-1})$, and is higher for lower l sublevels. Thus, high-l sublevels are depopulated more slowly relative to lower l sublevels on the same n level. This results in a slight increase in the departure coefficients. Reflecting the statistical weight factor in Equation 4.5, the higher l sublevels dominate the final b_n value resulting in an increase in the final b_n value. As the density increases, the l sublevels approach statistical distribution faster. As a result, the influence of the l sublevel population on the final b_n is larger for lower densities than for higher densities at a given T_e. The interplay of the rates produce the "bump" which is apparent in the b_n distribution (Figure 4.3)

The influence of l-changing collisions on the level populations and the resulting increase in the b_n values was already presented by Hummer and Storey (1987) and analyzed in detail by Strelnitski et al. (1996) in the context of hydrogen masers. The results of our level population models are in good agreement with those provided by Hummer and Storey (1987) as we show in Section 4.3.2.

4.3.1.2 Departure Coefficient for Carbon Atoms Including Dielectronic Recombination

Only carbon atoms recombining to the $^2P_{3/2}$ ion core are affected by dielectronic recombination. Having analyzed the departure coefficients for the hydrogenic case, we focus now on the $b_{nl}^{3/2}$ values and the resulting b_n^{final} as introduced in Section 4.2.1.

Figure 4.5 show example values for $b_n^{3/2}$ for $T_e = 50,\ 100,\ 200$ and $1000\ K$ and electron densities between 10^{-3} and 10^2 cm^{-3}. As pointed out by Watson

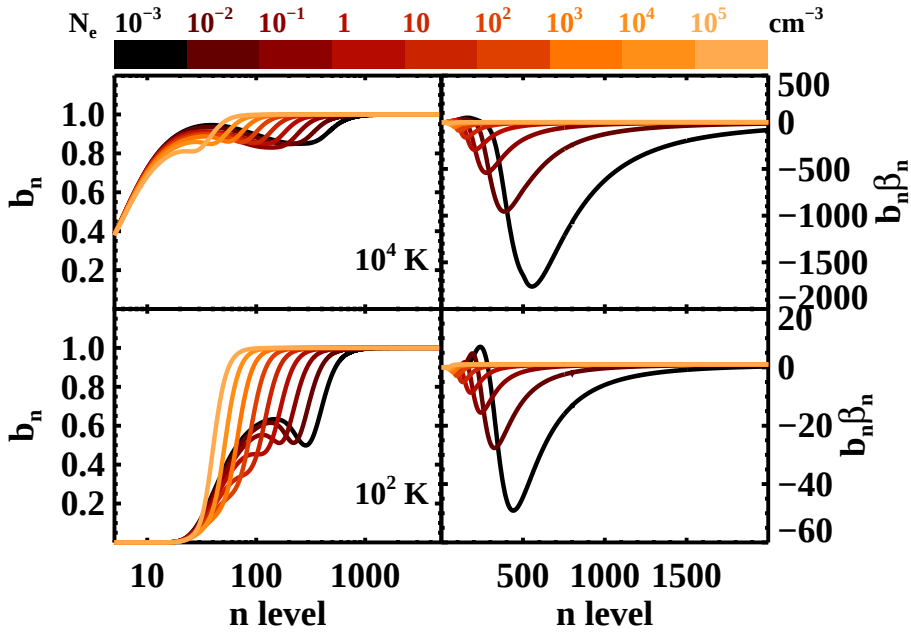

Figure 4.3: b_n values (left) and $b_n\beta_n$ values (right) for hydrogen at $T_e = 10^4$ and 10^2 K (upper and lower panels, respectively) for different densities (N_e, colorscale). The departure coefficients obtained using the nl-method show a "bump" at low n levels. The strength and position of the "bump" depend on the physical conditions. As density increases, the l-changing collisions redistribute the electron population more effectively.

et al. (1980), the low lying l sublevels are dominated by the dielectronic process and the $b_{nl}^{3/2}$ values are equal to b_{di} (Equation 4.27). As can be seen in Figure 4.1, such values can be much larger than unity at low densities resulting in an overpopulation of the low n levels for the 3/2 ion cores. In Figure 4.6 we show b_n^{final} as a function of n level under the same conditions. We see that at high electron densities the departure coefficients show a similar behavior as the hydrogenic values. Furthermore, an increase in the level population to values larger than unity is seen at low densities and moderate to high temperatures.

To guide the discussion, we analyze the behavior of the b_n^{final} when autoionization/dielectronic recombination dominates. This occurs at different levels depending on the values of T_e and N_e considered. Nevertheless, it is instructive to understand the behavior of the level population in extreme cases. When autoionization/dielectronic recombination dominate, the b_n^{final} in Equation 4.12

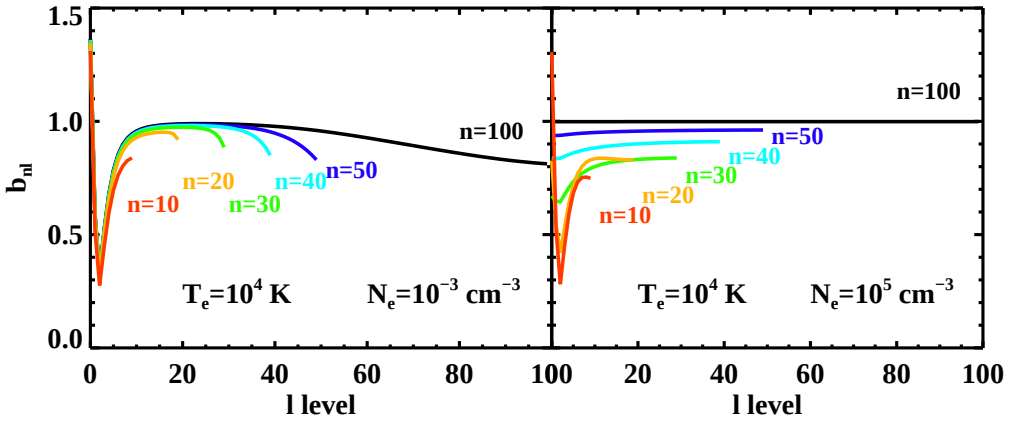

Figure 4.4: Example of hydrogenic b_{nl} values at low densities (*Left panel*) and high densities (*Right panel*). Statistical distribution of the l-sublevels is attained at levels as low as ~ 40. For lower levels, radiative processes dominate the level population. At low density (*Left panel*), radiative processes dominate even at high n levels.

is given by:

$$b_n^{final} \approx \frac{b_n^{1/2} + \left[N^+_{3/2}/N^+_{1/2}\right]_{LTE}}{1 + R\left[N^+_{3/2}/N^+_{1/2}\right]_{LTE}}. \tag{4.28}$$

At high densities, R approaches unity and we note two cases. The first case is when T_e is high, the maximum value of $\left[N^+_{3/2}/N^+_{1/2}\right]_{LTE} = 2$, meaning that a large fraction of the ions are in the $^2P_{3/2}$ core. Consequently, $b_n^{final} \approx (b_n^{1/2} + 2)/3$, thus the effect of dielectronic recombination is to increase the level population as compared to the hydrogenic case. We also note that since $b_n^{1/2} \leq 1$ the final $b_n^{final} \leq 1$. The second case we analyze is for low T_e, where

the ion LTE ratio is low and most of the ions are in the $^2P_{1/2}$ core. Thus, $b_n^{final} \approx b_n^{1/2}$ and the departure coefficients are close to hydrogenic.

At low densities, $R \ll 1$ and, as above, we study two cases. The first is when T_e is high, the maximum value of $\left[N^+_{3/2}/N^+_{1/2}\right]_{LTE} = 2$ and $b_n^{final} \approx b_n^{1/2} + 2$, therefore dielectronic recombination produces a large overpopulation as compared to the hydrogenic case. The second case is when T_e is low and most of the ions are in the $^2P_{1/2}$ level and, as in the high density case, the $b_n^{final} \approx b_n^{1/2}$. We note from this analysis that overpopulation of the b_n^{final} (relative to the hydrogenic case) is only possible for a range of temperatures and densities. In particular, b_n^{final} is maximum for high temperatures and low densities.

Having analyzed the behavior of the b_n^{final} values in the extreme $b_n^{3/2} = b_{di}$ case, now we analyze the behavior of $b_n^{3/2}$ with n. The population in the low n levels is dominated by dielectronic recombination (Watson et al., 1980; Walmsley and Watson, 1982a) and $b_n^{3/2} = b_{di}$ up until a certain n level where $b_n^{3/2}$ begins to decrease down to a value of one. The n value where this change happens depends on temperature, moving to higher n levels as T_e decreases. To understand this further, we analyze the rates involved in the l sublevel population (Figure 4.5). The low l sublevels are dominated by dielectronic recombination and autoionization and the b_{nl} values for the 3/2 ion cores are $b_{nl}^{3/2} = b_{di}$. For the higher l sublevels other processes (mainly collisions) populate or depopulate electrons from the level n and the net rate is lower than that of the low l dielectronic recombination/autoionization. This lowers the b_{nl} value, which is effectively delayed by l-changing collisions since they redistribute the population of electrons in the n level. The b_{nl} for highest l values dominate the value of $b_n^{3/2}$ due to the statistical weight factor.

We note that the behavior of the $b_n^{3/2}$ cores as a function of n (see Figure 4.7) can be approximated by:

$$b_n^{3/2} \approx \tanh\left(\left[\frac{l_m}{n}\right]^3\right) \times (b_{di} - 1) + 1. \tag{4.29}$$

with b_{di} defined as in Walmsley and Watson (1982a) (Equation 4.27) and l_m was derived from fitting our results:

$$l_m \approx 60 \times \left(\frac{N_e}{10}\right)^{-0.02} \left(\frac{T_e}{10^4}\right)^{-0.25} \tag{4.30}$$

In diffuse clouds the integrated line to continuum ratio is proportional to $b_n\beta_n$. We note that the β_n behavior is more complex as can be seen in Figure 4.8. The low n "bump" on the b_n^{final} makes the $b_n\beta_n$ high at low densities

and for levels between about 150 and 300. Since the b_n^{final} values decrease from values larger than one to approximately one, the β_n changes sign. In Figure 4.9 we show the electron density as a function of the level where the change of sign on the $b_n\beta_n$ occurs. At temperatures higher than about 200, our models for $N_e = 0.1$ cm^{-3} show no change of sign due to the combined effects of l-changing collisions and dielectronic recombination.

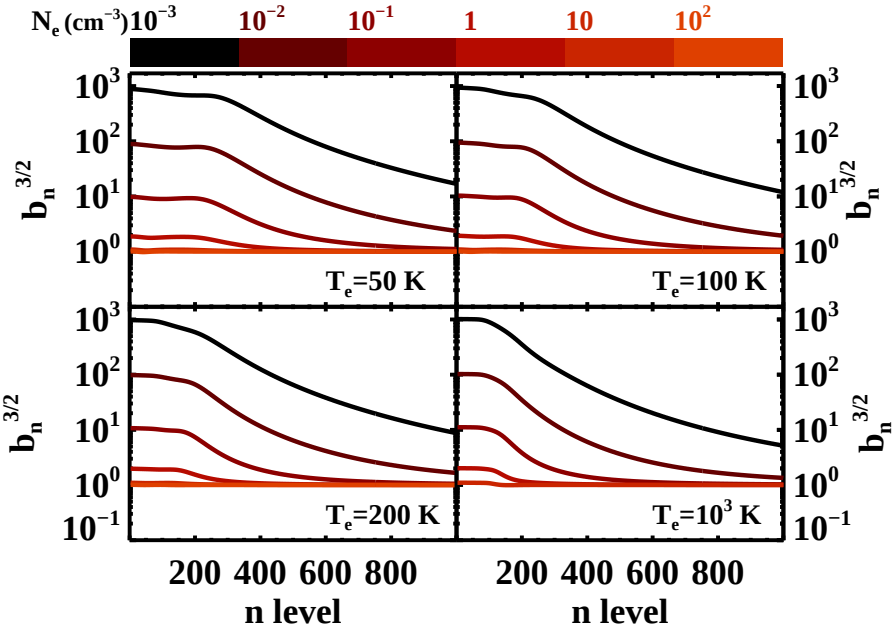

Figure 4.5: Departure coefficients for the $^2P_{3/2}$ parent ions as a function of n at $T_e = 50,\ 100,\ 200$ and 1000 K for different densities (N_e, colorscale). The values for low n levels are close to b_{di} and decrease towards a value of one. At high densities, $b_n^{3/2} \approx 1$.

4.3.2 Comparison with Previous Models

The level population of hydrogenic atoms is a well studied problem. Here, we will describe the effects of the updated collision rates as well as point out differences due to the improved numerical method.

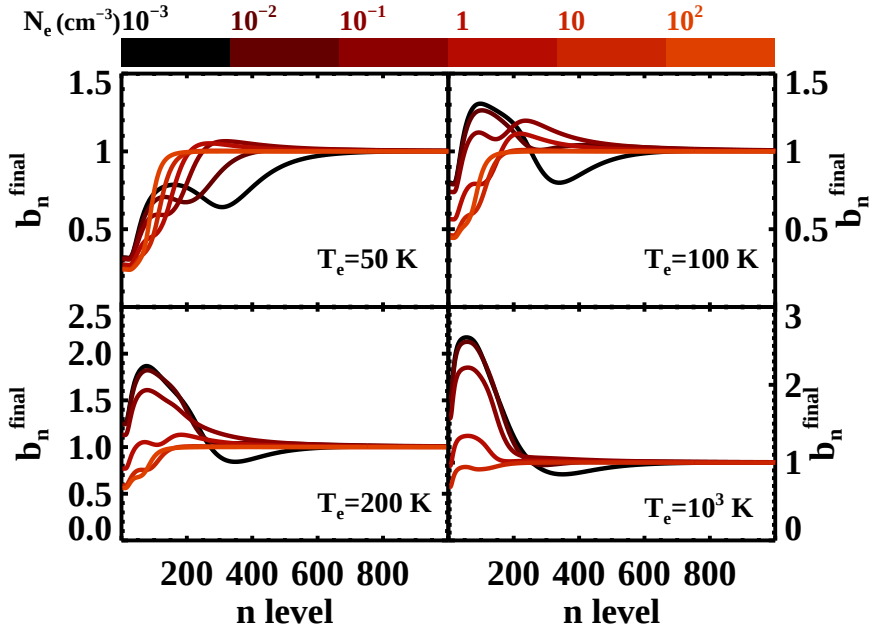

Figure 4.6: Final departure coefficients for carbon atoms (b_n^{final}) as a function of n level at T_e = 50, 100, 200 and 1000 K for different densities (N_e, colorscale). The "bump" seen in hydrogenic atoms is amplified by dielectronic recombination. As density increases the b_n^{final} are closer to the hydrogenic value.

4.3.2.1 Hydrogenic Atoms

At the lowest densities, we can compare our results for hydrogenic atoms with the values of Martin (1988) for Hydrogen atoms. The results of Martin (1988) were obtained in the low density limit, i.e. no collision processes were taken into account in his computations. The results are given in terms of the emissivity of the line normalized by the Hβ emissivity. As can be seen in Figure 4.10, our results agree to better than 5%, and for most levels to better than 0.5%.

At high densities, we compare the hydrogenic results obtained here with those of Hummer and Storey (1987). Our approach reproduces well the b_{nl} (and b_n) values of Hummer and Storey (1987) (to better than 1%) when using the same collision rates (Gee et al., 1976; Pengelly and Seaton, 1964) as can be seen in Figure 4.11. We note that the effect of using different energy changing rates ($C_{n,n'}$) has virtually no effect on the final b_n values. On the other hand, using

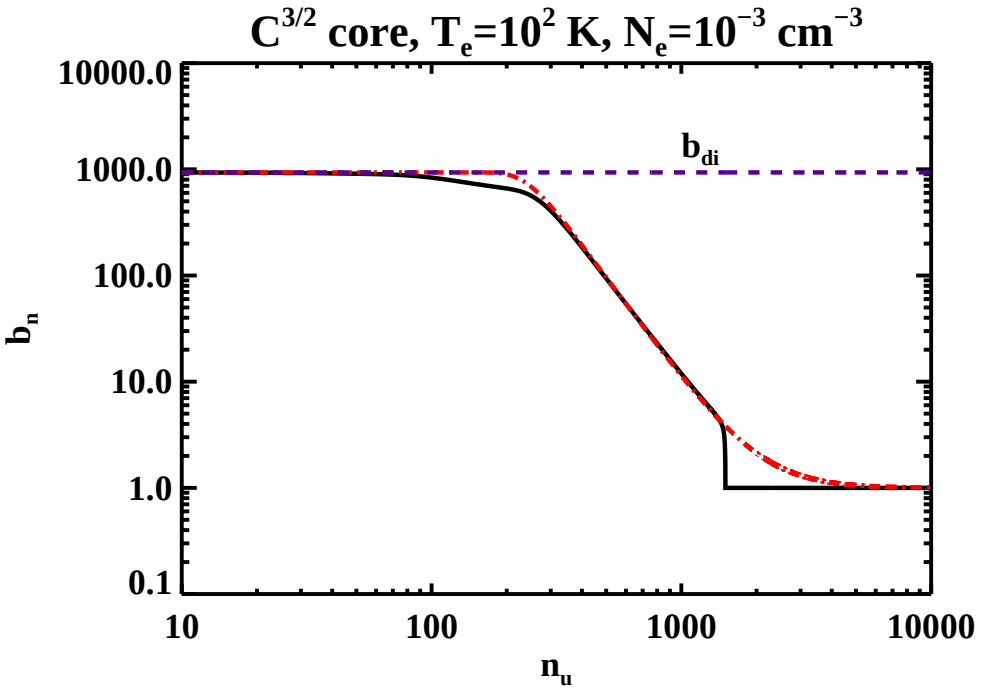

Figure 4.7: $b_n^{3/2}$ values for carbon as a black line (solid), the discontinuity at $n = 1500$ is due to the n_{crit} value. Overplotted as a red (dot dashed) line is the approximation in Equation 4.29. The blue (dashed) line is the value of b_{di}.

Vrinceanu et al. (2012) values for the $C_{nl,nl\pm1}$ rates results in differences in the b_n values of 5% at $T_e = 10^4$ K, $N_e = 100$ cm^{-3}. As expected, the difference is less at higher temperatures and densities since values are closer to equilibrium (see Figure 4.12). At low n levels, our results for high l levels are overpopulated as compared to the values of Hummer and Storey (1987) leading to an increases in the b_n values.

4.3.2.2 Carbon

Now we compare the departure coefficients obtained here with the results of Ponomarev and Sorochenko (1992). We focus the discussion on the b_n values from Ponomarev and Sorochenko (1992) as the Walmsley and Watson (1982a) values are similar. However, Walmsley and Watson (1982a) only present $b_n\beta_n$ plots and the values of β_n are quite sensitive to small changes in b_n. While the results presented here are remarkably different from those of Walmsley and Watson (1982a), some trends are similar.

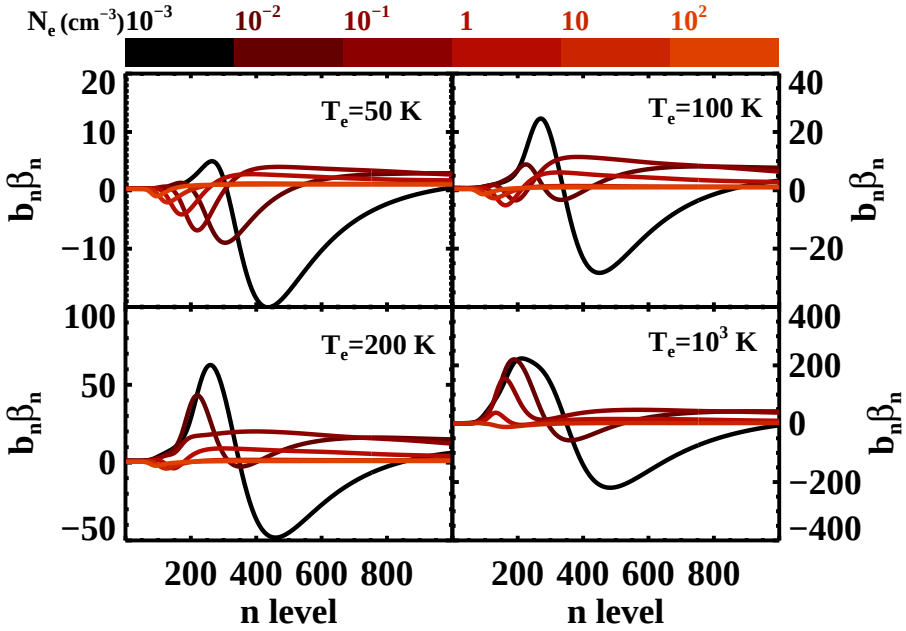

Figure 4.8: $b_n\beta_n$ values for carbon atoms at $T_e = 50,\ 100,\ 200$ and 1000 K for different densities (N_e, colorscale).

We start by comparing the departure coefficient presented here with those from Ponomarev and Sorochenko (1992) for the $T_e = 100$ K and at a density of $N_e = 0.1$ cm^{-3} (Figure 4.13). From the plots in Ponomarev and Sorochenko (1992) and using Equation 4.12 we can estimate the $b_n^{3/2}$ value [8]. At level $n = 100$ they give values of $b_n^{final} \sim 0.7$ and $b_n^{1/2} \sim 0.2$ from which we derive $b_n^{3/2} \sim 7$, which is 30% lower than our value of 10. Close to their peak in the b_n^{final} value, at $n = 400$, we derive from the plots a $b_n^{3/2} \sim 9$, while from our method we obtain a value closer to 3. Finally, at level $n = 900$, $b_n^{3/2} \sim 4$ from Ponomarev and Sorochenko (1992) and this is about a factor of two larger than our value.

The same exercise can be done for $N_e = 1$ cm^{-3}: for $n = 100,\ 300$ and 900 the $b_n^{3/2}$ calculated by Ponomarev and Sorochenko (1992) are $\sim 1.6,\ 1.8$ and 1, respectively. Our $b_n^{3/2}$ values are $\sim 2,\ 1.1$ and 1 for the same levels. At higher

[8] It is difficult to estimate the b_n value from the plots in Ponomarev and Sorochenko (1992) since the scale in their plots is not evenly spaced. We believe this might be due to a misprint and the values for $T_e = 100$ K were taken from Figure 2.35 in Gordon and Sorochenko (2009). For $T_e = 50$ K, we used the plots in Ponomarev and Sorochenko (1992).

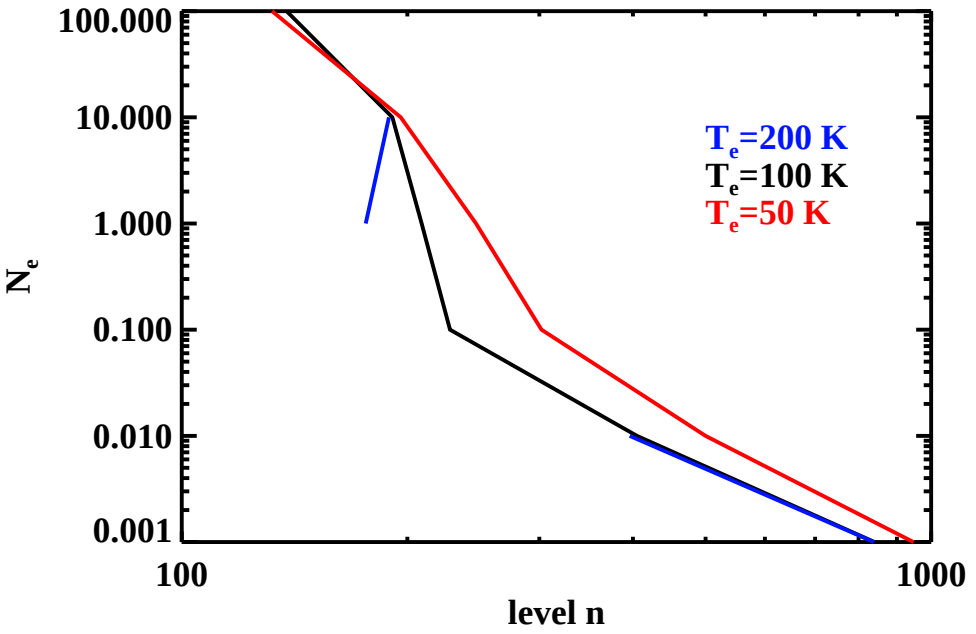

Figure 4.9: Level where the $b_n\beta_n$ values go to zero for $T_e = 50,\ 100$ and 200 K. At temperatures larger than 200 K and for an electron densities around 10^{-1} cm^{-3} the $b_n\beta_n$ values do not go through zero.

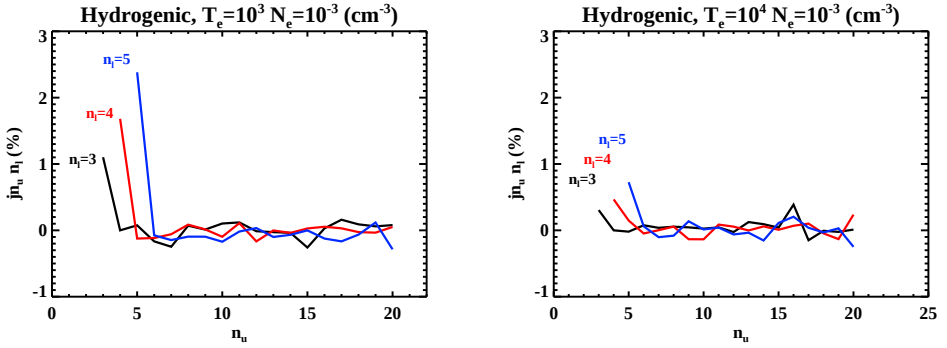

Figure 4.10: Difference between the emissivities (normalized to Hβ) for low nl lines at low density and the results from Martin (1988) in the low N_e approximation. Our results agree to better than 1% at most levels.

densities, our results are similar to the hydrogenic case and agree with Ponomarev and Sorochenko (1992). This is expected, as discussed in Section 4.3.1

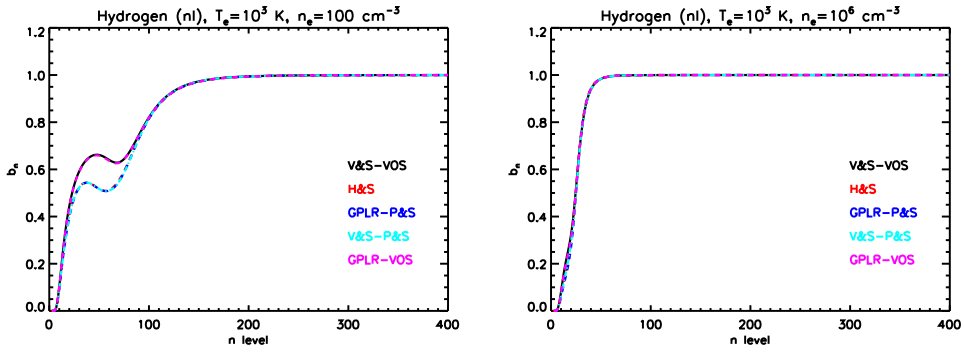

Figure 4.11: A comparison of the effect of different collision rates on the final b_n values for $T_e = 100$ K and $N_e = 100$ and 10^6 cm^{-3}. H&S are the departure coefficients from Hummer and Storey (1987) who used Gee et al. (1976); GPLR corresponds to the use of n changing collision rates from Gee et al. (1976), V&S from Vriens and Smeets (1980); P&S corresponds to the use of l-changing collision rates from Pengelly and Seaton (1964), VOS corresponds to Vrinceanu et al. (2012). The largest differences are $\sim$ 30% due to the use of different l-changing collision rates.

at high densities b_n values approach equilibrium.

At lower temperatures, we analyze the case of $T_e = 50$ K. For $N_e = 0.1$ cm^{-3}, the $b_n^{3/2}$ values derived from the Ponomarev and Sorochenko (1992) plots are: 8, 7, and 3 for levels $n = 100,\ 400$ and 900, respectively (cf. Figure 4.13). The values derived from our models are 10, 7, and 1, for the same levels (Figure 4.5). At $N_e = 1$ cm^{-3}, Ponomarev and Sorochenko (1992) find $\sim 1.6,\ 1.6$ and 1 for these levels and our values are quite similar. As a general trend, our values at $n \approx 100$ are similar to those from Ponomarev and Sorochenko (1992). At this level, dielectronic recombination and autoionization dominate the rates in the level population equation and the $b_n^{3/2}$ are close to b_{di}. At higher levels, the Ponomarev and Sorochenko (1992) values remain close to b_{di} while our values decrease. It seems that the influence of dielectronic processes in Ponomarev and Sorochenko (1992) remain important at higher n levels than in our simulations. We attribute this discrepancy to the use of different collision rates. Indeed, at high densities the differences become smaller since the levels approach collisional equilibrium.

Differences in the b_n^{final} values obtained here and those given in Ponomarev and Sorochenko (1992) produce discrepancies in the β_n values. For high n levels, our values can differ by an order of magnitude when compared to those of Ponomarev and Sorochenko (1992). For example, at level $n = 900$, the $b_n\beta_n$ value from Ponomarev and Sorochenko (1992) is $\sim$ 100 for the $T_e =$

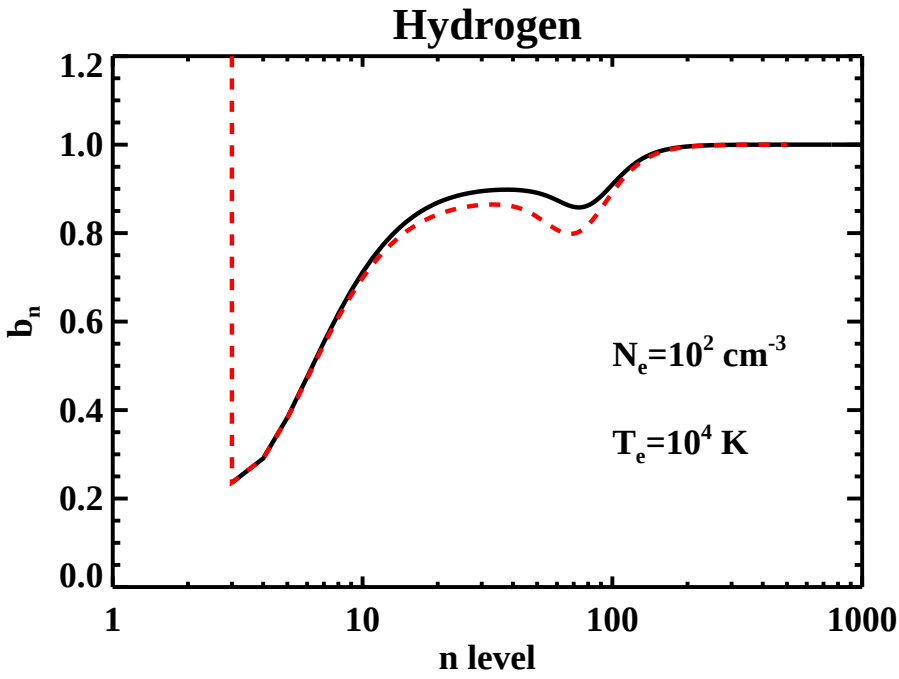

Figure 4.12: Comparison between our b_n values (black) at $T_e = 10^4$ K and $N_e = 100$ cm^{-3} and the results from Hummer and Storey (1992) (red line, dashed). Differences are due to the use of l-changing collision rates from Vrinceanu et al. (2012).

100 K, $N_e = 0.1$ cm^{-3} case. Using $b_n = 1.2$ and Equation 4.6, we estimate the ratio $b_{n+1}/b_n = 0.9996$ for the results in Ponomarev and Sorochenko (1992). Our result is ~ 0.99997 for the same physical conditions. The β_n values are quite sensitive to small variations in b_n^{final}. Since our b_n^{final} values are quite different from those in Ponomarev and Sorochenko (1992), large differences in the β_n values are not surprising.

4.4 Summary and Conclusions

We have solved the level population equation for hydrogenic atoms using accurate rates involved in the process. The level population equation is solved in two approximations: the n and the nl method. The departure coefficients obtained using the n method are similar to values from the literature (e.g. Brocklehurst 1970 and Shaver 1975). Our results using the nl method reproduce those from Hummer and Storey (1987) well, once allowance is made for updates in the

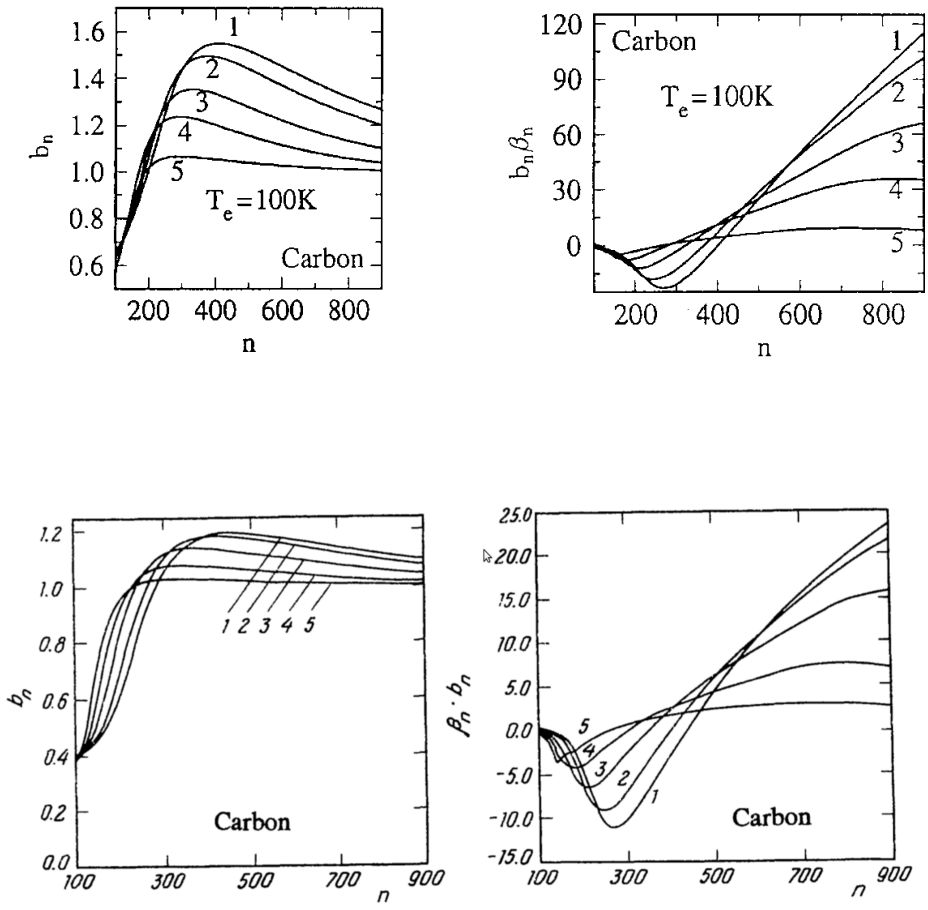

Figure 4.13: Departure coefficients from Ponomarev and Sorochenko (1992) at T_e = 100 K and 50 K. Lines correspond to electron densities n_e = 0.05, 0.1, 0.3, 1.0 and 3.0 cm^{-3} marked from 1 to 5 (from lower to higher densities). Upper panels: b_n values (Left) and $b_n\beta_n$ values for T_e = 100 K (Gordon and Sorochenko, 2009). Lower panels: b_n values (Left) and $b_n\beta_n$ values for T_e = 50 K (Ponomarev and Sorochenko, 1992).

collisional rates.

By including the dielectronic recombination process together with the *nl* method we are able to model the level population of carbon in terms of the departure coefficients. Our results are qualitatively similar to those of Watson

et al. (1980); Walmsley and Watson (1982a). However, the values obtained here differ considerably from those from the literature. The differences can be understood in terms of the use of improved collision rates and the improved numerical approach using the nl method. We confirm that dielectronic recombination can indeed produce an increase on the values of the departure coefficients at high n levels compared to the hydrogenic values.

In anticipation of low frequency radio recombination line surveys of the diffuse interstellar medium now being undertaken by LOFAR, we have expanded the range of applicability of the formulation to the conditions of the cold neutral medium. For this environment, external radiation fields also become important at intermediate principal quantum levels while at high levels the influence of radiation fields on the level population is less important. In Section 5, we discuss the expected line strength for low frequency carbon radio recombination lines. We compare our results to existing observations of CRRLs towards Cas A and regions in the inner galaxy. We also describe the analysis techniques and diagnostic diagrams that can be used to analyze the forthcoming LOFAR CRRL survey. The departure coefficients obtained here will be used to analyze the LOFAR observations of Cas A in a future article (Oonk et al., 2015a).

A List of Symbols

Table 4.1: List of Symbols

Symbol	Descritpion
$A_{3/2,1/2}$	Spontaneous transition rate of the carbon fine structure line $^2P_{3/2}$-$^2P_{1/2}$
A^a_{nl}	Autoionization rate
$A_{n'n}$	Einstein coefficient for spontaneous transition between n' and n
$A_{n'l'nl}$	Einstein coefficient for spontaneous transition between $n'l'$ state to nl state
a_0	Bohr radius
a_{nl}	Photoionization cross section
$B_{nn'}$	Einstein coefficient for stimulated transition from level n' to n
b_n	Departure coefficient for level n
$b_n^{1/2}$	Departure coefficient for atoms recombining from the 1/2 ion core for level n
$b_n^{3/2}$	Departure coefficient for atoms recombining from the 3/2 ion core for level n
b_n^{final}	Departure coefficient for atoms recombining from both ion cores
C$n\alpha$	Carbon recombination line for α transition
$C_{n'n}$	Rates for energy changing collisions between level n' and n
$C(n,l)$	Coefficient for recursion relations used to obtain the radial matrices values
c	Speed of light
$EM_{\mathrm{C+}}$	Emission measure of carbon ions
$g_{3/2}$	Statistical weight for the fine structure level $^2P_{3/2}$
$g_{1/2}$	Statistical weight for the fine structure level $^2P_{1/2}$
h	Planck constant
$I_0(\nu)$	Intensity of the background continuum
I_ν^{line}	Intensity of the line
I_ν^{cont}	Intensity of the continuum
I_{158}	Intensity of the fine structure line of carbon at 158 μm
j_ν	line emission coefficient
k_ν	line absorption coefficient
k	Boltzmann constant

Continued on next page

Table 4.1 – *Continued from previous page*

Symbol	
L	Pathlength of cloud
l	Angular momentum quantum number
N_{cr}	Critical density for collisions on a two level atom
N_n	Density of atoms in level n
N_{nl}	Density of atoms in level n and sublevel l
N_e	Electron density
N_H	Hydrogen density
N_{ion}	Density of the parent ions
$N^+_{3/2}$	Level population of carbon ions in the $^2P_{3/2}$ core
$N^+_{1/2}$	Level population of carbon ions in the $^2P_{1/2}$ core
n	Lower principal quantum number
n'	Upper principal quantum number
n_{max}	Maximum level considered in our simulations
n_{crit}	Critical level considered in our simulations for the nl-method
n_t	Level where observed lines transition from emission to absorption
$\mathscr{R}(n,l)$	Normalized radial wave function for level n, l
R	Ratio between the fine structure ($^2P_{3/2}$-$^2P_{1/2}$) level population and the fine structure level population in LTE
$R(l',l)$	Integral of the radial matrix elements
Ry	Rydberg constant
T_0	Temperature of power law background spectrum at frequency ν_0
T_e	Electron temperature
Z	
α_n	Radiative recombination coefficient to a level n
α_{nl}	Radiative recombination coefficient to a level n and sublevel l
α^d_{nl}	Dielectronic recombination rate
$\beta_{nn'}$	Correction factor for stimulated emission
γ_e	De-excitation rate for carbon ions in the $^2P_{3/2}$ core due to collisions with electrons
γ_H	De-excitation rate for carbon ions in the $^2P_{3/2}$ core due to collisions with hydrogen atoms
ΔE	Energy difference between two levels
Δn	$n'-n$, difference between the upper an lower principal quantum number
η	Correction factor to the Planck function due to non-LTE level population

Continued on next page

Table 4.1 – *Continued from previous page*

Symbol	
μ	Reduced mass
ν	Frequency of a transition
ν_0	Reference frequency for the power law background spectrum
$\phi(\nu)$	Line profile
ω_{nl}	Statistical weight of level nl
ω_i	Statistical weight of parent ion
χ_n	Ionization potential of a level n, divided by kT_e

B Level population

The strength (or depth) of an emission (absorption) line depends on the level population of atoms. The line emission and absorption coefficients are given by (e.g. Shaver 1975; Gordon and Sorochenko 2009):

$$j_\nu = \frac{h\nu}{4\pi} A_{n'n} N_{n'} \phi(\nu), \tag{B1}$$

$$k_\nu = \frac{h\nu}{4\pi} \left(N_n B_{nn'} - N_{n'} B_{n'n}\right) \phi(\nu), \tag{B2}$$

where h is the Planck constant, $N_{n'}$ is the level population of a given upper level (n') and N_n is the level population of the lower level (n); $\phi(\nu)$ is the line profile, ν is the frequency of the transition and $A_{n'n}$, $B_{n'n}(B_{nn'})$ are the Einstein coefficients for spontaneous and stimulated emission (absorption), respectively. Following Hummer and Storey (1987), we present the results of our modeling in terms of the departure coefficients (b_n) and the correction factor for stimulated emission/absorption (β_n):

$$b_n = \frac{N_n}{N_n(LTE)}. \tag{B3}$$

$$\beta_{n,n'} = \frac{1 - (b_{n'}/b_n)\exp(-h\nu/kT_e)}{1 - \exp(-h\nu/kT_e)}, \tag{B4}$$

unless otherwise stated the β_n presented here correspond to $\beta_{n+1,n}$, i.e. α transitions. When a cloud is located in front of a strong background source the integrated line to continuum ratio is proportional to $b_n\beta_n$ (Shaver, 1975; Payne et al., 1994). We expand on the radiative transfer problem in Paper II.

B.1 Hydrogenic atoms

Under thermodynamic equilibrium conditions, level populations are given by the Saha-Boltzmann equation (e.g. Brocklehurst and Seaton 1972; Gordon and Sorochenko 2009):

$$N_{nl}(LTE) = N_e N_{ion} \left(\frac{h^2}{2\pi m_e k T_e} \right)^{3/2} \frac{\omega_{nl}}{2\omega_i} e^{\chi_n}, \chi_n = \frac{hcZ^2 Ry}{n^2 k T_e}, \quad \text{(B5)}$$

where N_e is the electron density in the nebula, N_{ion} is the ion density, m_e is the electron mass, k is the Boltzmann constant, Ry is the Rydberg constant ω_{nl} is the statistical weight of the level n and angular quantum momentum level l [$\omega_{nl} = 2(2l+1)$, for hydrogen], ω_i is the statistical weight of the parent ion. The factor $\left(h^2/2\pi m_e k T_e\right)^{0.5}$ is the thermal de Broglie wavelength, Λ, of the free electron $\left[\Lambda(T_e)^3 \approx 4.14133 \times 10^{-16}\ T_e^{-1.5}\ \mathrm{cm}^3\right]$. In general, lines are formed under non-LTE conditions and, in order to properly model the line behavior, the level population equation must be solved. We follow the methods described in Brocklehurst (1971) and improved upon by Hummer and Storey (1987) as described in Section 4.2. Here, we give a detailed derivation of the theory and methods. First, we solve the level population equation assuming statistical population of the angular momentum l-levels, i.e.:

$$N_n = \sum_{l=0}^{n-1} \frac{(2l+1)}{n^2} N_{nl}, \quad \text{(B6)}$$

for all n levels. This assumption greatly simplifies the calculations but is only valid when l changing transitions are faster than other processes, and, in general, this is not the case for low n levels. The level population equation under this assumption is (e.g. Shaver 1975; Gordon and Sorochenko 2009):

$$N_n \left[\sum_{n'<n} A_{nn'} + \sum_{n' \neq n} (B_{nn'} I_\nu + C_{nn'}) + C_{ni} \right] =$$
$$\sum_{n'>n} N_{n'} A_{n'n} + \sum_{n' \neq n} N_{n'} (B_{n'n} I_\nu + C_{n'n}) + N_e N_{ion} (\alpha_n + C_{in}). \quad \text{(B7)}$$

The right- and left-hand side of Equation B7 describe how level n is populated and depopulated, respectively. We take into account spontaneous transitions from level n to lower levels ($A_{nn'}$), stimulated emission and absorption ($B_{nn'} I_\nu$, $B_{n'n} I_\nu$), collisional transitions ($C_{nn'}$), radiative recombination (α_n), collisional ionization (C_{in}) and 3-body recombination (C_{ni}). Equation B7 can be written

in terms of the departure coefficients (b_n):

$$b_n \left[\sum_{n'<n} A_{nn'} + \sum_{n' \neq n} (B_{nn'} I_\nu + C_{nn'}) + C_{ni} \right] = \sum_{n'>n} b_{n'} \frac{\omega_{n'}}{\omega_n} e^{\Delta\chi_{n'n}} A_{n'n} + \sum_{n' \neq n} b_{n'} \frac{\omega_{n'}}{\omega_n} e^{\Delta\chi_{n'n}} (B_{n'n} I_\nu + C_{n'n}) + \frac{N_e N_{ion}}{N_n(LTE)} (\alpha_n + C_{in}). \quad \text{(B8)}$$

The previous equation can be written as a matrix equation of the form $\mathbf{R}\times\mathbf{b}=\mathbf{S}$ by choosing the appropriate elements to form the matrices $\mathbf{R}$ and $\mathbf{S}$ (e.g. Shaver 1975):

$$R_{n'n} = -\frac{\omega_{n'}}{\omega_n} e^{\Delta\chi_{n'n}} (A_{n'n} + B_{n'n} I_\nu + C_{n'n}), (n' > n) \quad \text{(B9)}$$

$$R_{nn} = \sum_{n'<n} A_{nn'} + \sum_{n' \neq n} (B_{nn'} I_\nu + C_{nn'}) + C_{ni} \quad \text{(B10)}$$

$$R_{n'n} = -\frac{\omega_{n'}}{\omega_n} e^{\Delta\chi_{n'n}} (B_{n'n} I_\nu + C_{n'n}), (n' < n) \quad \text{(B11)}$$

$$S_n = \frac{N_e N_{ion}}{N_n(LTE)} (\alpha_n + C_{in}). \quad \text{(B12)}$$

It is easy to solve for the b_n values by using standard matrix inversion techniques. We will refer to this approach of solving the level population equation as the n-method.

At low n levels, the quantum angular momentum distribution must be obtained, since the assumption that the angular momentum levels are in statistical equilibrium is no longer valid. Moreover, as described in Watson et al. (1980); Walmsley and Watson (1982a), dielectronic recombination is an important process for carbon ions at low temperatures and densities. Since the dielectronic recombination process depends on the quantum angular momentum distribution, we need to include the l sublevel distribution for a given n level.

The level population equation considering l-levels is:

$$b_{nl} \left[\sum_{n'<n} \sum_{l'=l\pm1} A_{nln'l'} + \sum_{n' \neq n} (B_{nln'l'} I_\nu + C_{nln'l'}) + \sum_{l'=l\pm1} C_{nlnl'} + C_{nl,i} \right] = \sum_{n'>n} \sum_{l'=l\pm1} b_{n'l'} \frac{\omega_{n'l'}}{\omega_{nl}} e^{\Delta\chi_{n'n}} A_{n'l'nl} + \sum_{n' \neq n} \sum_{l'=l\pm1} b_{n'l'} \frac{\omega_{n'l'}}{\omega_{nl}} e^{\Delta\chi_{n'n}} (B_{n'l'nl} I_\nu + C_{n'l'nl}) + \sum_{l'=l\pm1} b_{nl'} \left(\frac{\omega_{nl'}}{\omega_{nl}} \right) C_{nl'nl} + \frac{N_e N_{ion}}{N_{nl}(LTE)} (\alpha_{nl} + C_{i,nl}). \quad \text{(B13)}$$

To solve for the l level distribution at a given n level we followed an iterative approach as described in Brocklehurst (1971); Hummer and Storey (1987). We will refer to this approach of solving the level population equation as the nl-method.

We start the computations by applying the n-method, i.e. assuming $b_{nl} = b_n$ for all l levels, thus obtaining $b_{nl}^{(0)}$ values. For levels above a given n_{crit} value we expect the l-sublevels to be in statistical equilibrium. In this case, Equation B6 is valid and the b_{nl} values are equal to those obtained by the n-method. On the first iteration, we start solving Equation B13 at $n = n_{crit}$ and use the previously computed values ($b_{n'l'}^{(0)}$) for levels $n' \neq n$. Equation B13 is then a tri-diagonal matrix (only elements with $l' = l \pm 1$, enter in the equation) and, by solving the system of equations, we obtain $b_{nl}^{(1)}$ values. The operation is repeated for all n levels down to $n = n_{min}$. In all our simulations we assume $n_{min} = 3$ since we are focused on studying carbon atoms whose ground level correspond to $n = 2$. We repeat the operation by using the $b_{nl}^{(1)}$ values instead of the $b_{nl}^{(0)}$ values. Hummer and Storey (1987) have proven that considering collisions from (and to) all n' levels guarantees a continuous distribution between both approaches at levels close to n_{crit}. The final b_n values are computed by taking the weighted sum of the b_{nl} values:

$$b_n = \sum_{l=0}^{n-1} \left(\frac{2l+1}{n^2} \right) b_{nl}, \tag{B14}$$

Details on the parameters used in this work are given in the text (Section 4.2.2).

C Radial Matrices and Einstein A coefficients

In general, the radiative decay depends on the angular momentum quantum number of the electron at the level n. Transitions from level $nl \rightarrow n'l'$ are described by $A_{nln'l'}$ coefficients, in the dipole approximation (Seaton, 1959a):

$$A_{nln'l'} = \frac{64\pi^4\nu^3}{3hc^3} e^2 a_0^2 \frac{\max(l,l')}{2l+1} \left| \int_0^\infty \mathscr{R}(n',l') r \mathscr{R}(n,l) \mathrm{d}r \right|^2, \tag{C1}$$

where a_0 is the Bohr radius and $\mathscr{R}(n,l)$ is the normalized radial wave function solution to the Schrödinger equation of the Hydrogen atom (Burgess, 1958; Brocklehurst, 1971). The computation of the matrix elements is challenging (see Morabito et al. 2014c for details) and we follow the recursion relations given by Storey and Hummer (1991) to calculate them up to $n = 10000$. Defining:

$$R(l',l) = \int_0^\infty \mathscr{R}(n',l') r \mathscr{R}(n,l) \mathrm{d}r, \tag{C2}$$

where the first argument of $R(l',l)$ corresponds to the lower state. For a given n' level, Storey and Hummer (1991) give the following relations, with the starting values:

$$\begin{aligned} R(n',n'-1) &= 0, \\ R(n'-1,n') &= \frac{1}{4}\left(4nn'\right)^{n'+2}\left[\frac{(n+n')!}{(n-n'-1)!(2n'-1)!}\right]^{1/2}\frac{(n-n')^{n-n'-2}}{(n+n')^{n+n'+2}}. \end{aligned}$$

The recursion relations are:

$$2lC(n',l)R(l-1,l) = (2l+1)C(n,l+1)R(l,l+1) + C(n',l+1)R(l+1,l), \quad \text{(C3)}$$

and:

$$2lC(n,l)R(l,l-1) = C(n,l+1)R(l,l+1) + (2l+1)C(n',l+1)R(l+1,l), \quad \text{(C4)}$$

with:

$$C(n,l) = \frac{\sqrt{(n+l)(n-l)}}{nl} \quad \text{(C5)}$$

D Radiative recombination cross-section

Storey and Hummer (1991) give a formula for computing the photoionization cross-section:

$$a_{nl}(h\nu) = \left(\frac{4\pi a_0^2\alpha}{3}\right)\frac{\left(1+n^2\kappa^2\right)}{\mu^2 Z^2 n^2}\frac{\max(l,l')}{2l+1}\left|\int_0^\infty \mathscr{R}(n',l')r\mathscr{R}(\kappa,l)\mathrm{d}r\right|^2. \quad \text{(D1)}$$

To obtain the radial matrices elements, we use the same recursion formula as for the Einstein A coefficients with the substitution: $n = i/\kappa$, with i the imaginary number. The $C(n,l)$ coefficients are:

$$C(n,l) = \frac{\sqrt{(1+l^2\kappa^2)}}{l}, \quad \text{(D2)}$$

and the initial values are:

$$\begin{aligned} R(n',n'-1) &= 0, \\ R(n'-1,n')_{\kappa=0} &= \frac{1}{4}\left[\frac{\pi}{2\,(2n'-1)!}\right]^{1/2}(4n')^{n'+2}e^{-2n'}, \\ R(n'-1,n')_{\kappa\neq 0} &= \left[\frac{\prod_{s=1}^{n'}(1+s^2\kappa^2)}{1-\exp(-2\pi/\kappa)}\right]^{1/2}\frac{\exp[2n'-(2/\kappa)\arctan(n'\kappa)]}{\left(1+n'^2\kappa^2\right)^{n'+2}}R(n'-1,n')_{\kappa=0}. \end{aligned}$$

We are interested in computing the recombination cross-section for an electron with energy E recombining to a level nl. From Milne relation we obtain (e.g. Rybicki and Lightman 1986):

$$\sigma(E,nl) = \frac{16\pi a_0^2}{3\sqrt{2}}\sqrt{\frac{hcRy}{E}}\sqrt{\frac{m_e c^2}{E}}\left(\frac{E+h\nu_n}{m_e c^2}\right)^3 \sum_{l'} \max(l,l') \left| \int_0^\infty \mathscr{R}(\kappa,l') r \mathscr{R}(n,l) \mathrm{d}r \right|^2 \quad \text{(D3)}$$

expressed in terms of the radial matrices. Here, $h\nu_n$ is the ionization energy of the level n. The final rate is obtained by integrating the cross-section over a Maxwellian velocity distribution:

$$\alpha_{nl} = \frac{8}{\sqrt{\pi m_e}}(kT_e)^{-3/2} \int_0^\infty \sigma(E,nl) e^{-E/kT_e} \mathrm{d}E. \quad \text{(D4)}$$

We consider $x = E/kT_e$ and $I(x)$ is the function in the integral. To integrate the cross-section, we followed an approach similar to Burgess (1965). We divide the integral in 30 segments starting at $x_0 = kT \times 10^{-10}$, and ending at $x_f = 20 \times kT$. Each segment is integrated by using a 6-point Gauss-Legendre quadrature scheme. This approach provides the value of the integral close to kT, therefore two correction factors must be applied: for the small values of x we note that the integrand is almost constant and the value of the integral is then $I(x_0)x_0^2/2$; for large values of x we use a 6-point Gauss-Legendre quadrature starting at $x_0 = 20 \times kT$ and ending at $x_f = 30 \times kT$. As mentioned in Section 4.3 we compare the sum over l, of our radiative recombination rates with the formula of Seaton (1959b):

$$\alpha_n = 2.06 \times 10^{-11} \left(\frac{Z}{nT_e^{0.5}}\right) \chi_n S_n(\lambda) \ \mathrm{cm^3 s^{-1}}, \quad \text{(D5)}$$

with $\lambda = n^2\chi_n$, and

$$S_n(\lambda) = \int_0^\infty \frac{g_{II}(n,\epsilon)e^{-x_n u}}{1+u} du, u = n^2\epsilon. \quad \text{(D6)}$$

Values for the $\chi_n S_n(\lambda)$ are given by Seaton (1959b) in two approximations for large and small argument, and tabulated values are also given for values in between the approximations. A first order expansion of the Gaunt factor (Allen, 1973) provides an accurate formula for the recombination coefficient:

$$\alpha_n = 3.262 \times 10^{-6} \left(\frac{Z^4}{n^3 T_e^{1.5}}\right) e^{\chi_n} E_1(\chi_n) \ \mathrm{cm^3 s^{-1}}. \quad \text{(D7)}$$

E Energy changing collision rates

Vriens and Smeets (1980) obtained the following semi-empirical formula for excitation by electrons. The formula is given by:

$$C_{nn'} = 1.6 \times 10^{-7} \frac{\sqrt{kT_e}}{kT_e + \Gamma_{nn'}} \exp(-\epsilon_{nn'}) \left[A_{nn'} \ln(0.3 \frac{kT_e}{hcRy} + \Delta_{nn'}) + B_{nn'} \right], \quad \text{(E1)}$$

with the coefficients defined as:

$$\begin{aligned}
s &= |n - n'|, \\
A_{nn'} &= 2 \frac{hcRy}{E_{nn'}} f_{nn'}, \\
B_{nn'} &= 4 \frac{(hcRy)^2}{n^3} \left(\frac{1}{E_{nn'}^2} + \frac{4}{3} \frac{E_{ni}}{E_{nn'}^3} + b_p \frac{E_{ni}^2}{E_{nn'^4}} \right), \\
b_p &= 1.4 \frac{\ln(n)}{n} - \frac{0.7}{n} - \frac{0.51}{n^2} + \frac{1.16}{n^3} - \frac{0.55}{n^4}, \\
\Delta_{nn'} &= \exp(-\frac{B_{nn'}}{A_{n,n'}}) + 0.06 \frac{s^2}{nn'^2},
\end{aligned}$$

$$\Gamma_{nn'} = hcRy \ln(1 + \frac{n'^3 kT_e}{hcRy}) \left[3 + 11 \left(\frac{s}{p} \right)^2 \right] \left(6 + 1.6ns + \frac{0.3}{s^2} + 0.8 \sqrt{\frac{n^3}{s}} \, |s - 0.6| \right)^{-1}.$$

F Collisional ionization

We use the formulation in the code of Brocklehurst and Seaton (1972) to obtain the values for the collisional ionization rates, the formulation is based on Burgess and Percival (1968):

$$C_{i,n} = \frac{5.444089}{T_e^{3/2}} e^{-\chi_n} \left[\left(\frac{5}{3} - \frac{\chi_n}{3} \right) \frac{1}{\chi_n} + \frac{1}{3} (\chi_n - 1) E_1(\chi_n) e^{\chi_n} - \frac{1}{2} E_1(\chi_n)^2 e^{2\chi_n} \right], \quad \text{(F1)}$$

in units of cm^3 s^{-1}.